Weak First-Order Tilting Transition in Monolayers of Mono- and Bipolar Docosanol Derivatives†

Xiuli Yue,‡ Bodo Dobner,§ Ken-ichi Iimura,|| Teiji Kato,|| Helmuth Möhwald,‡ and Gerald Brezesinski*,‡

Max Planck Institute of Colloids and Interfaces, Research Campus Golm, Am Muehlenberg 1, D-14476 Potsdam, Germany, Institute of Pharmaceutical Chemistry, Martin Luther University, D-06120 Halle/S., Germany, and Department of Applied Chemistry, Faculty of Engineering, Utsunomiya University, 7-1-2 Yoto, Utsunomiya 321-8585, Japan

Received: November 9, 2005; In Final Form: January 17, 2006

A systematic analysis of pressure−area isotherms and grazing incidence X-ray diffraction (GIXD) data of 22-methoxydocosan-1-ol ($H_3C-O-(CH_2)_{22}-OH$, MDO), docosan-1-ol ($H_3C-(CH_2)_{21}-OH$, DO), and docosyl methyl ether ($H_3C-(CH_2)_{21}-O-CH_3$, DME) monolayers on pure water between 10 and 35 °C is presented. All monolayers form fully condensed phases in the investigated temperature region. The GIXD data reveal that the monolayers exhibit the phase sequence $L_2'-S$ at lower temperature and $L_2'-LS$ at higher temperature. Phase diagrams have been established. Inserting a second hydrophilic group at the opposite end of the molecule (bipolar MDO) shifts the S/LS boundary to higher temperatures. All monolayers exhibit herringbone (HB) packing at lower temperatures. The "kink" in the isotherms observed at lower temperatures is replaced by a very small plateau region at higher temperatures. The entropy changes connected with this weak first-order tilting transition are much smaller compared with the first-order transition from liquid-expanded (LE) to condensed (LC). Additionally, this transition is endothermic in contrast to the LE/LC transition. The reason for the endothermic transition is the weaker positional correlation in the nontilted state compared with the tilted one. The appearance of the weak first-order endothermic transition can be connected with the changed phase sequence. X-ray photoelectron spectroscopy (XPS) measurements provide information about the polar group orientation. Considerations based on GIXD and XPS data as well as adhesion energy of the different terminal end groups lead to the conclusion that the hydroxyl group of the bipolar MDO is attached to the water surface while the methoxy group is in contact with air. The presented results show that the second hydrophilic group influences the monolayer properties in a mild way.

1. Introduction

Langmuir monolayers of simple fatty alcohols have been extensively studied by surface pressure isotherm experiments, optical methods, and grazing incidence X-ray diffraction at the air−water interfaces.[1−7] Long-chain alcohol monolayers exhibit a defined number of structural phase transitions. For this reason, the phase diagram of fatty alcohols is as generic as that of fatty acids, since other single-chain amphiphiles reproduce either one or the other phase diagram, depending on the effective headgroup size of the molecules.[8]

On the other hand, inserting a second polar group in lipids allows modification of the competitive interaction of hydrophobic and hydrophilic parts of the amphiphiles.[9−11] Bipolar amphiphiles are important for understanding structure and function of special biological and reconstituted membranes. The lipids of archaebacteria membranes, which differ strongly in structure and function from those of procaryotes and eukaryotes, enable the existence of these organisms under drastic living conditions.[12,13] Archaebacterial lipids possess branched chains, which are bound via ether linkage to glycerol at *sn*-2,3-configuration. Whereas the lipids of halophilic bacteria are monopolar lipids, the methanogens and thermoacidophiles are mainly bipolar with membrane-spanning chains.[14−17] Because of the great potential of these lipids in biotechnology, material science, and pharmacology, the characterization of natural archaebacterial lipids and also of model compounds is of great importance.[18−20] Monolayer investigations of lipids in general have shown the value of this method in membrane research, especially in modeling interactions with membrane surfaces. However, the monolayer behavior of bipolar compounds is still a problem. On compression, the formation of a layer with upright oriented chains has been reported, whereupon one polar headgroup is attached to water and the other is exposed to air.[21−23] Other authors have found a horseshoe-like arrangement, in which both polar groups have contact with the water surface.[24−26] The coexistence of both conformations has been also reported.[27] The upright orientation of bipolar compounds seems to be strongly dependent on the polarity and size of the headgroups. Therefore, the monolayer behavior of a bipolar compound with the smallest possible headgroups has been investigated and compared with the corresponding monopolar amphiphiles. The hydroxyl group is the simplest hydrophilic group with the smallest cross-sectional area, and the change from hydroxyl to acid group is drastic. The second polar group with a different hydrophilicity is the methoxy group. Monolayer

† Part of the special issue "Charles M. Knobler Festschrift".
‡ Max Planck Institute of Colloids and Interfaces.
§ Martin Luther University.
|| Utsunomiya University.

10.1021/jp056482o CCC: $33.50
Published on Web 02/24/2006

studies of ethers are comparatively rare, and most investigations are concentrated on lipids with ether linkages.[28−30]

In this paper, the bipolar amphiphile 22-methoxydocosan-1-ol ($H_3C-O-(CH_2)_{22}-OH$, MDO) and the monopolar amphiphile docosyl methyl ether ($H_3C-(CH_2)_{21}-O-CH_3$, DME) have been selectively synthesized for the first time as model compounds to elaborate the effect of a second polar group on the monolayer behavior by comparison with the corresponding alcohol docosan-1-ol ($H_3C-(CH_2)_{21}-OH$, DO). The longer chain length has the advantage that the monolayer is completely insoluble and more stable at the air−water interface. The monolayer structures of amphiphilic docosanol derivatives at the air−water interface were studied by grazing incidence X-ray diffraction (GIXD). X-ray photoelectron spectroscopy (XPS) was applied to the transferred monolayer of the bipolar amphiphile in order to confirm the orientation of the hydrophilic end groups in the condensed monolayer state. Only in very few cases could this question be answered directly.[31,32]

2. Experimental Section

2.1. Materials. Docosan-1-ol ($H_3C-(CH_2)_{21}-OH$, DO) was purchased from Sigma (approximately 99%) and used without further purification. The spreading solvent was chloroform obtained from Merck. 22-Methoxydocosan-1-ol ($H_3C-O-(CH_2)_{22}-OH$, MDO) and docosyl methyl ether ($H_3C-(CH_2)_{21}-O-CH_3$, DME) were synthesized according to the following procedures.

22-Methoxy-1-(tetrahydro-2H-pyran-2-yloxy)-docosan. A quantity (2.3 mmol, 56.3 mg) of NaH (60% in mineral oil) was washed with dry ether to remove the mineral oil. Then, the sodium hydride was suspended in 15 mL toluene. Pure, dried 22-(tetrahydro-2*H*-pyran-2-yloxy)-docosan-1-ol[33,34] (2.3 mmol, 1 g) was added to the slurry. After completion of the deprotonation (15−24 h), 3.3 mmol (478 mg) methyl iodide and a catalytic amount of tetrabutylammonium iodide were added. The mixture was then heated under reflux with stirring for 40 h. The mixture was washed three times with 15 mL water, dried over sodium sulfate, and evaporated to dryness. The compound was purified by column chromatography on silica gel 60 (Merck) using heptane/ether 98:2. Yield: 530 mg (52%) white solid, mp 38−39 °C. MS *m*/*z*: 439 [$M^+ - H$]. ^{1}H NMR (400 MHz, $CDCl_3$, δ): 1.18−1.27 (m, 36H, $-CH_2-$ chain); 1.47−1.60 (m, 8H, −CH2−, ring, chain); 1.68−1.84 (m, 2H, $O-CH_2-CH_2-CH_2-$); 3.3 (s, 3H, $-OCH_3$); 3.32−3.49 (m, 4H, $-CH_2-CH_2-O-$); 3.67−3.73 (m, 1H, $-CH_2-O-CH-$); 3.82−3.88 (m, 1H, $-CH_2-O-CH-$); 4.54−4.56 (m, 1H, $-O-CH-O-$). ^{13}C NMR (100 MHz, $CDCl_3$, δ): 19.58−30.71 (ring, chain); 30.9 ($-CH_2-CH-$, ring); 58.46 ($-O-CH_3$); 62.3 ($-CH_2-O-CH-$); 67.68 ($-CH-O-CH_2-$); 72.98 ($-CH_2-O-CH_3$); 98.9 (−O-*C*H−O-). Elemental analysis: found C, 76.36; H, 12.48; calcd C, 76.30; H, 12.11.

22-Methoxy-docosan-1-ol ($H_3C-O-(CH_2)_{22}-OH$, MDO). A quantity (1.1 mmol, 485 mg) of 22-methoxy-1-(tetrahydro-2*H*-pyran-2-yloxy)-docosan was dissolved in 40 mL methanol. After addition of a catalytic amount of pyridinium tosylate, the mixture was heated under reflux for 5 h. The reaction mixture was then concentrated under reduced pressure to 10−15 mL; 50 mL ether and 30 mL water were added, and the mixture was shaken. The etheral phase was separated, dried (sodium sulfate), and evaporated to dryness. The crude product was purified by column chromatography on silica gel 60 using the gradient technique (heptane/$CHCl_3$, 50/50 to 30/70). Yield: 328 mg (83.6%) white solid, mp 66−68 °C. MS *m*/*z* (ESI): 379 [$M^+ - Na$]. ^{1}H NMR ($CDCl_3$, 400 MHz, δ): 1.18−1.32 (m, 38H, $-CH_2-CH_2-CH_2-$, chain); 1.5−1.57 (m, 2H, $-O-CH_2-CH_2-CH_2-$); 3.3 (s, 3H, $-O-CH_3$), 3.3−3.36 (t, $J = 6.835$, 2H, $-CH_2-O-CH_3$); 3.59−3.63 (t, $J = 6.64$, 2H, $HO-CH_2-$). ^{13}C NMR ($CDCl_3$, 100 MHz, δ): 25.64 ($HO-CH_2-CH_2-CH_2-$); 26.03 ($CH_3-O-CH_2-CH_2-CH_2-$); 29.34−29.58 (chain); 32.74 ($HO-CH_2-CH_2-$); 58.46 (CH_3-O-); 63.1 ($HO-CH_2-CH_2-$); 72.98 ($CH_3-O-CH_2-CH_2-$). Elemental analysis: found C, 77.35; H, 13.49; calcd C, 77.46; H, 13.57.

Docosyl-methyl-ether ($H_3C-(CH_2)_{21}-O-CH_3$, DME). A quantity (10 mmol, 3.26 g) of docosan-1-ol was added to a suspension of 10 mmol (0.24 g) NaH in 30 mL THF with stirring at room temperature. After the hydrogen evolution was finished, 30 mmol (84.26 g) methyl iodide was dropped into the slurry. The mixture was heated and kept for 8 h at 50 °C. Then, the mixture was diluted with 50 mL ether and washed twice with 30 mL water. The etheral phase was dried (sodium sulfate) and evaporated under vacuum. The substance was purified by column chromatography using heptane/chloroform (9/1 to 6/4) and finally by crystallization from heptane. Yield: 2.86 g (84%) white crystals, mp 47.5−48 °C. MS *m*/*z*: 339 [$M^+ - H$]. ^{1}H NMR ($CDCl_3$, 400 MHz, δ): 0.91 (t, 3H, $-CH_3$); 1.20−1.35 (m, 40H, chain); 3.30 (s, 3H, $-O-CH_3$); 3.35 (t, 2H, $-CH_2-CH_2-O-$). ^{13}C NMR ($CDCl_3$, 100 MHz, δ): 14.32 ($-CH_3$), 22.73 ($-CH_2-CH_3$), 26.2−32.05 (chain), 58.5 ($-O-CH_3$), 73.0 ($-CH_2-CH_2-O-$). Elemental analysis: found C, 81.08; H, 14.04; calcd C, 81.10; H, 14.21.

2.2. Film Balance Measurements. Surface pressure area isotherms ($\pi-A$ isotherms) were measured on a Teflon trough (Riegler & Kirstein, Potsdam, Germany). The surface pressure was recorded with a continuous Wilhelmy-type pressure measuring system using a filter paper as plate with accuracy better than 0.1 $mN \cdot m^{-1}$. The substances were spread from 1 mM chloroform solution onto the water surface using a 100-μL syringe. The monolayers were compressed at a rate of 5 $Å^2 \cdot molecule^{-1} \cdot min^{-1}$ after about 10 min of solvent evaporation. All experiments were performed using ultrapure water obtained from a Millipore system with a specific resistance above 18 $M\Omega \cdot cm$ as the subphase.

2.3. X-ray Photoelectron Spectroscopy (XPS). XPS is one of the most extensively used techniques for surface analysis because of its high sensitivity to the chemical structure near the surface (0.5−8 nm). Orientation of the polar end groups of the bipolar amphiphilic molecules in condensed monolayers was evaluated by XPS takeoff angle (TOA) dependency experiments.[35] The monolayer of MDO was deposited on RCA-cleaned silicon wafer substrates by the vertical dipping method at 27 $mN \cdot m^{-1}$ and 20 °C. The silicon wafer was immersed into water before monolayer spreading. The XPS measurement was performed using a Physical Electronics ESCA 5600 spectrometer with a monochromatic Al Kα X-ray source (1486.6 eV) operated at 14 kV and 150 W. The pressure in the sample chamber was maintained at about 3×10^{-8} Pa during the measurement. The XPS C1s spectra were measured in the high-resolution mode (0.125 eV/step, 58.7 eV pass energy, large Omni focus lens area) at TOAs of 80°, 70°, 58°, 45°, 33°, 20°, 10°, and 5° at different positions on the sample surface. Gauss functions are fitted to the experimental data for spectra deconvolution. The spectra energy scale was calibrated with the C−H peak at 284.6 eV.

2.4. Grazing Incidence X-ray Diffraction (GIXD). Grazing incidence X-ray diffraction was performed using the liquid-surface diffractometer on the undulator beamline BW1 at HASYLAB, DESY, Hamburg, Germany.[36−40]

A monochromatic beam was adjusted to strike the surface with an angle of incidence of $0.85\alpha_c$ ($\alpha_c = 0.13°$ is the critical angle for total reflection). The intensity of the diffracted beam is detected by a linear position-sensitive detector (PSD) (OED-100-M, Braun, Garching, Germany) as a function of the vertical scattering angle α_f. The resolution of 0.09° of the horizontal scattering angle 2θ is given by a Soller collimator located in front of the PSD. According to the geometry of diffraction, the scattering vector **Q** has an in-plane component $Q_{xy} = 2\pi/\lambda$ ($\cos^2 \alpha_i + \cos^2 \alpha_f - 2 \cos \alpha_i \cos \alpha_f \cos 2\theta)^{1/2}$ and an out-of plane component $Q_z = 2\pi/\lambda(\sin \alpha_i + \sin \alpha_f)$. The accumulated position-resolved scans were corrected for polarization, footprint area, and powder-averaging (Lorentz factor). Model peaks taken to be Lorentzian in the in-plane direction and Gaussian in the out-of-plane direction were fitted to the corrected intensities. The lattice spacings are obtained from the in-plane diffraction data. The lattice parameters can be calculated from the lattice spacings.

The positional correlation length ξ can be estimated from the full width at half-maximum (fwhm) of the Bragg peaks. For an exponential decay of positional correlation as observed in liquid crystals (corresponding to a Lorentzian as a Bragg peak profile), it is $\xi = 2/\text{fwhm}(Q_{xy})$.[41]

3. Results and Discussion

3.1. Pressure−Area Isotherms. The lateral pressure as a function of the area per molecule ($\pi-A$ isotherm) has been measured at different temperatures. The $\pi-A$ isotherms of DME (docosyl methyl ether, $H_3C-(CH_2)_{21}-O-CH_3$), DO (docosan-1-ol, $H_3C-(CH_2)_{21}-OH$), and MDO (22-methoxydocosan-1-ol, $H_3C-O-(CH_2)_{22}-OH$) indicate that all samples form only condensed monolayer phases in the investigated temperature region. Figure 1 shows typical isotherms. At lower temperatures, the $\pi-A$ isotherms of the monopolar DME (Figure 1a) exhibit a change of slope (kink) typical for a second-order transition from a tilted to a nontilted state. This phase transition pressure shifts first to slightly higher values with increasing subphase temperature (from 14.5 $mN\cdot m^{-1}$ at 15 °C to 18.4 $mN\cdot m^{-1}$ at 25 °C) and then decreases again on further temperature increase (13.7 $mN\cdot m^{-1}$ at 30 °C and 10.6 $mN\cdot m^{-1}$ at 35 °C). The isotherms show clearly that the transition kink observed at lower temperatures is replaced by a small plateau at higher temperatures. Such a small plateau may be attributed to a weak first-order phase transition.

Assuming that the phase transition pressure π_t is approximately linearly dependent on the subphase temperature, a temperature coefficient of -0.67 $mN\cdot m^{-1}\cdot K^{-1}$ can be calculated for the high-temperature transition. On the basis of this result, a transition enthalpy was calculated by the area change during the phase transition applying a modified Clausius−Clapeyron equation: $d\pi_t/dT = \Delta H/T(A_u - A_t)$, where π_t is the transition pressure at the temperature T, A_u is the molecular area in the nontilted phase at π_t, and A_t is the molecular area in the tilted phase at π_t. The transition enthalpy is positive because of the negative temperature dependence of the transition pressure and the negative $\Delta A = (A_u - A_t)$ value. It amounts to 0.428 $kJ\cdot mol^{-1}$ at 30 °C and to 0.844 $kJ\cdot mol^{-1}$ at 35 °C. These values are rather small compared with the values of the transition from the liquid-expanded (LE) to condensed (LC) state, and this transition is endothermic in contrast to the LE−LC transition.

The $\pi-A$ isotherms of the simple alcohol DO show a similar behavior. Again, the phase transition pressure from a tilted to a nontilted state depends on the subphase temperature and goes trough a maximum at around 28 °C. At higher temperatures,

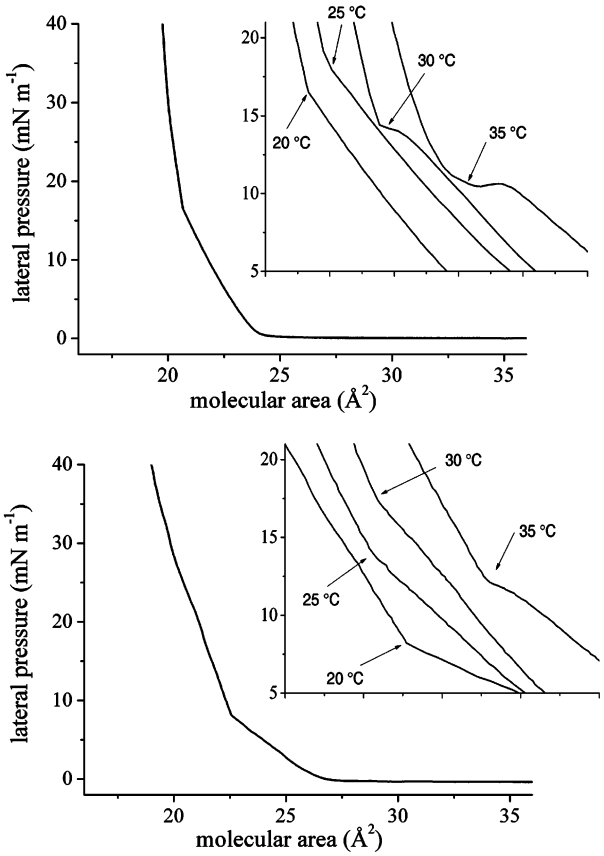

Figure 1. $\pi-A$ isotherms of DME (docosyl methyl ether, $H_3C-(CH_2)_{21}-O-CH_3$) (top) and MDO (22-methoxydocosan-1-ol, $H_3C-O-(CH_2)_{22}-OH$) (bottom) at 20 °C. The insert shows an extended view for pressures between 5 $mN\cdot m^{-1}$ and 21 $mN\cdot m^{-1}$ and for a small range of molecular areas. The isotherms are shifted in area for clarity. Depending on the temperature, the appearance of kinks or plateaus in the isotherms is clearly visible.

the isotherms exhibit again a kind of plateau region instead of a clear kink. Taking into account that the increase of the chain length by 4 methylene groups on going from octadecanol to docosanol is equivalent to a temperature decrease of 20−24 °C, one expects the S−LS transition between 28 °C and 32 °C for DO.[42] Indeed, the isotherms at and above 30 °C show features known for octadecanol, e.g., the transition pressure into the nontilted phase decreases just above the S−LS transition.

The addition of the corresponding second hydrophilic group to the opposite end of DO or DME leads to the bipolar molecule MDO. This bipolar substance shows an identical film behavior (Figure 1). The kink in the isotherms indicates again a second-order phase transition from a tilted to a nontilted state. On increasing temperature from 15 °C to 30 °C, the phase transition pressure first increases to 18 $mN\cdot m^{-1}$ and then decreases to 12.5 $mN\cdot m^{-1}$ at 35 °C, where the plateau appears. It is remarkable that no additional transition is observed in the isotherms that might be attributed to a change in molecular orientation from both ends grafted to the water surface to one end grafted only.

The question arises whether the observed temperature behavior of the transition pressure and the change from a second-order to a weak first-order transition is directly connected with a changed phase sequence. Therefore, GIXD experiments have been performed.

3.2. GIXD Measurements. GIXD experiments were performed at different temperatures to elucidate the monolayer phase structures of DME, DO, and MDO. Selected contour plots

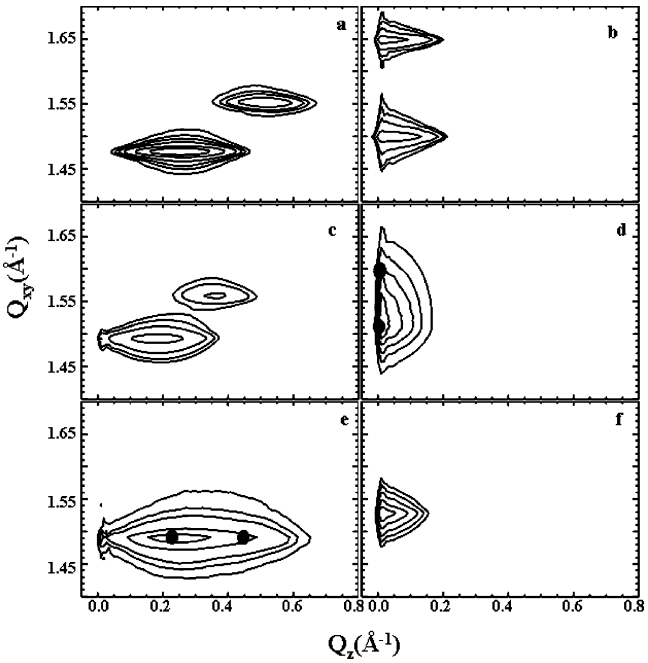

Figure 2. Contour plots of the diffracted intensities as a function of the in-plane scattering vector component Q_{xy} and the out-of-plane scattering vector component Q_z for monolayers of DME (docosyl methyl ether, $H_3C-(CH_2)_{21}-O-CH_3$): 7 mN·m^{-1} (a) and 20 mN·m^{-1} (b) at 20 °C; 7 mN·m^{-1} (c) and 20 mN·m^{-1} (d) at 27 °C; 7 mN·m^{-1} (e) and 20 mN·m^{-1} (f) at 32 °C. The fitted peak positions are marked in (d) and (e) to make the figure clear despite the strong overlap of the peaks.

(corrected intensities as a function of the in-plane, Q_{xy}, and out-of-plane, Q_z, components of the scattering vector) of DME are shown in Figure 2. The corresponding Bragg peak and Bragg rod maxima are presented in Table 1. At lower surface pressure, the DME monolayer exhibits two Bragg peaks at nonzero Q_z values. The Q_z maxima are in a 2:1 ratio. Such an intensity distribution is characteristic for the orthorhombic L_2' phase with the molecules tilted into the next-nearest-neighbor (NNN) direction.[43] The structure at low pressure is independent of the subphase temperature. On compression, both peaks move to higher Q_{xy} and lower Q_z positions, indicating that the tilt angle decreases. The unit cell is distorted in the direction to the nearest neighbor (NN). At higher pressures, both peaks are located at zero Q_z, indicating a vertical orientation of the molecules in the orthorhombic S phase at 20 °C and 27 °C (Figure 2b and d). According to the isotherms, the phase transition $L_2'-S$ is a second-order phase transition. At 27 °C, the two Bragg peaks are very broad, indicating a loss in position correlation. A linear dependence of the lattice distortion d on $\sin^2(t)$ is observed at lower temperatures (Figure 3). A d_0 value, which is significantly different from zero, indicates an ordering of the zigzag planes of the chains. The decreasing absolute value of d_0 on increasing temperature is an indication for the approaching S−LS transition. For a second-order transition, a linear relationship between $\sin^2(t)$ and the lateral pressure π is expected.[44] A linear dependence follows also from the simple approximation that the molecular area depends linearly on the lateral pressure, $A_{xy} = K_1 - K_2\pi$. Then, $1/\cos(t)$ must be also linearly dependent on π, because the tilt angle is related to the molecular area according to the equation: $\cos(t) = A_0/A_{xy}$, where A_0 is the cross-sectional area of the molecule, which is assumed to be dependent on temperature but independent of π at a constant pressure. The cross-sectional area of DME increases continuously on increasing temperature from 18.7 Å^2 at 10 °C to 19.6 Å^2 at 32 °C. The lateral pressure at which a packing of upright oriented chains should be obtained can be derived from an extrapolation to zero tilt angle. The extrapolated phase transition pressures are 15.9 mN·m^{-1} at 20 °C and 16.5 mN·m^{-1} at 27 °C. These values agree well with the data derived from the isotherms. At 32 °C, the two Bragg peaks observed in the tilted phase at lower pressures merge into one peak at higher pressure, indicating a hexagonal symmetry of the lattice. Such a diffraction pattern is typical for the LS phase. At 32 °C and low lateral pressures, the lattice is undistorted. Therefore, one expects that on further increasing the temperature the lattice distortion direction will change to NNN. This would indicate a transition from the L_2' into the Ov phase (NNN tilt and NNN distortion), which is a rotator phase, on increasing the temperature. The much larger cross-sectional area is an additional sign for this approaching transition. According to the pressure−area isotherms measured at 30 and 35 °C, the Ov (L_2')−LS transition is a weak first-order phase transition.

TABLE 1: Data Derived from GIXD Measurements of DME between 10 and 32 °C

T (°C)	π (mN m^{-1})	Q_{xy} (Å^{-1})	Q_z (Å^{-1})	a (Å)	b (Å)	A_0 (Å^2)	A_{xy} (Å^2)	tilt	d
10	0	1.511	0	5.00	7.48	18.7	18.7	0	−0.1468
		1.681	0						
12	0	1.507	0.115	5.00	7.53	18.7	18.9	7.9	−0.1387
		1.667	0.230						
14	0	1.468	0.305	5.02	8.18	19.1	20.6	21.7	−0.0604
		1.535	0.610						
	2	1.475	0.270	5.02	8.03	19.1	20.2	19.0	−0.0796
		1.564	0.541						
	6	1.506	0	5.03	7.48	18.8	18.8	0	−0.1507
		1.680	0						
20	1	1.462	0.327	5.00	8.39	19.2	21.0	23.6	−0.0318
		1.497	0.655						
	4	1.468	0.293	5.00	8.26	19.3	20.7	21.1	−0.0487
		1.522	0.586						
	7	1.477	0.257	5.00	8.10	19.2	20.2	18.4	−0.0671
		1.552	0.515						
	10	1.484	0.208	5.00	7.94	19.2	19.9	14.9	−0.0870
		1.582	0.420						
	13.5	1.493	0.131	5.00	7.76	19.2	19.4	9.5	−0.1108
		1.619	0.27						
	20	1.50	0	5.01	7.63	19.1	19.1	0	−0.1291
		1.648	0						
27	3	1.470	0.293	4.96	8.44	19.5	20.9	21.6	−0.0172
		1.489	0.588						
	7	1.479	0.241	4.96	8.25	19.4	20.4	18.1	−0.0396
		1.523	0.498						
	11	1.492	0.184	4.94	8.06	19.3	19.9	13.6	−0.0612
		1.561	0.378						
	19.9	1.514	0	4.87	7.92	19.3	19.3	0	−0.0629
		1.586	0						
32	7.5	1.489	0.223	4.872	8.44	19.7	20.6	16.9	0
		1.489	0.452						
	20	1.527	0	4.75	8.23	19.6	19.6	0	0

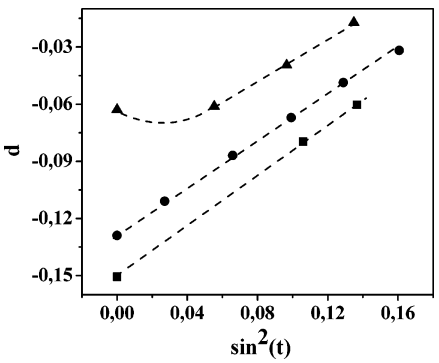

Figure 3. Distortion d as function of $\sin^2(t)$, where t is the tilt angle to the normal, for DME (docosyl methyl ether, $H_3C-(CH_2)_{21}-O-CH_3$) at 14 °C (■), 20 °C (●), and 27 °C (▲).

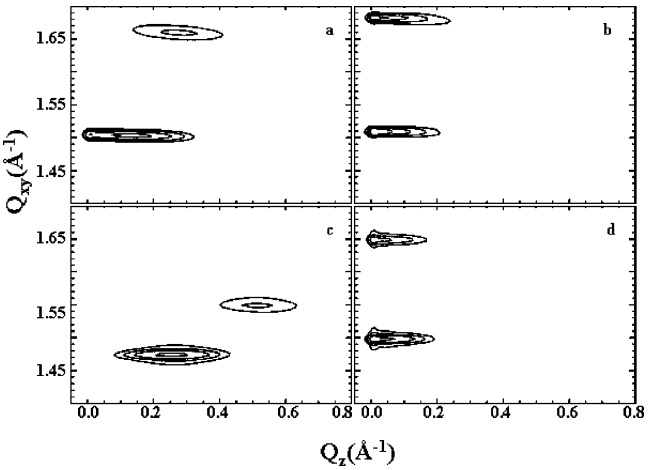

Figure 4. Contour plots of diffracted intensities vs in-plane scattering vector component Q_{xy} and out-of-plane scattering vector component Q_z for monolayers of DO (docosan-1-ol, $H_3C-(CH_2)_{21}-OH$): 0.8 mN·m^{-1} (a) and 3.9 mN·m^{-1} (b) at 10 °C; 6.7 mN·m^{-1} (c) and 22.0 mN·m^{-1} (d) at 20 °C.

TABLE 2: Data Derived from GIXD Measurements of DO at 10 and 20 °C

T (°C)	π (mN m^{-1})	Q_{xy} (Å^{-1})	Q_z (Å^{-1})	a (Å)	b (Å)	A_0 (Å^2)	A_{xy} (Å^2)	tilt	d
10	0.8	1.503	0.135	5.01	7.53	18.7	19.0	9.3	−0.1365
		1.660	0.271						
	1.9	1.506	0.095	5.01	7.52	18.7	18.9	6.4	−0.1431
		1.671	0.189						
	3.9	1.509	0	5.01	7.47	18.7	18.7	0	−0.1495
		1.682	0						
20	1	1.464	0.308	5.01	8.31	19.3	20.8	22.2	−0.0435
		1.512	0.617						
	3.7	1.469	0.287	5.01	8.22	19.3	20.6	20.5	−0.0541
		1.529	0.572						
	6.7	1.474	0.262	5.01	8.11	19.2	20.3	18.7	−0.0672
		1.549	0.524						
	10.6	1.481	0.219	5.01	7.99	19.3	20.0	15.5	−0.0845
		1.576	0.436						
	16.3	1.492	0.131	5.01	7.76	19.2	19.5	9.2	−0.1117
		1.619	0.262						
	22.8	1.498	0	5.02	7.61	19.1	19.1	0	−0.1319
		1.649	0						

A similar phase behavior was found in DO monolayers. At lower lateral pressure, two well-resolved diffraction peaks at $Q_z > 0$ reveal that the monolayer forms the rectangular L_2' phase (Figure 4, Table 2). Upon increasing pressure, these two diffraction peaks move to zero Q_z, indicating the formation of the S phase above 2.8 mN·m^{-1} at 10 °C and above 19.5 mN·m^{-1} at 20 °C. Since Q_{xy} of the nondegenerate peak is larger than that of the degenerate peak, the lattice is distorted in the NN direction. The cross-sectional area increases from 18.7 Å^2 at 10 °C to 19.2 Å^2 at 20 °C. These values are almost identical to the A_0 values of DME, indicating that both the alcohol and methyl ether headgroups are small and allow tight packing of the molecules. Therefore, in addition, the distortion of the unit cell is very similar for both molecules (Figure 5).

In comparison with DO and DME monolayers, the diffraction data for MDO (Figure 6 and Table 3) show that the transition from L_2' to LS occurs at 7 mN·m^{-1} (20 °C) and at 14.1 mN·m^{-1} (26 °C). Again, an increase of the second-order phase transition pressure with increasing temperature is observed. The tilt direction is NNN, and the distortion direction is NN. The extrapolation of the plots of d versus $\sin^2(t)$ to zero tilt angle yields nonzero d_0 values at 20 and 26 °C, indicating that the lattice distortion is caused by two factors: the tilting of the molecules and the ordering of the zigzag planes of the chains (Figure 7). At 35 °C, the diffraction patterns are noisy because of condensation of water vapor on the Capton window of the trough container. However, it is clear from the diffraction pattern that the molecules are tilted in the NNN direction and that the lattice is distorted in the NN direction at lower pressure, indicating that MDO forms the L_2' phase. Around 15 mN·m^{-1}, the molecules are nontilted and hexagonally packed, indicated by the appearance of a single Bragg peak at zero Q_z. This peak has again a large fwhm showing that the structure is weakly ordered. Therefore, lattice distortion at lower pressures is caused by both the tilting of the molecules and the backbone ordering of the chains. This chain order is lost at the transition into the weakly ordered nontilted LS phase.

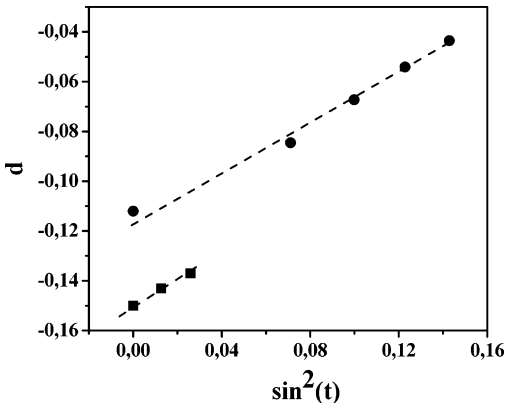

Figure 5. Distortion d as function of $\sin^2(t)$, where t is the tilt angle to the normal, for DO (docosan-1-ol, $H_3C-(CH_2)_{21}-OH$) at 10 °C (■) and 20 °C (●).

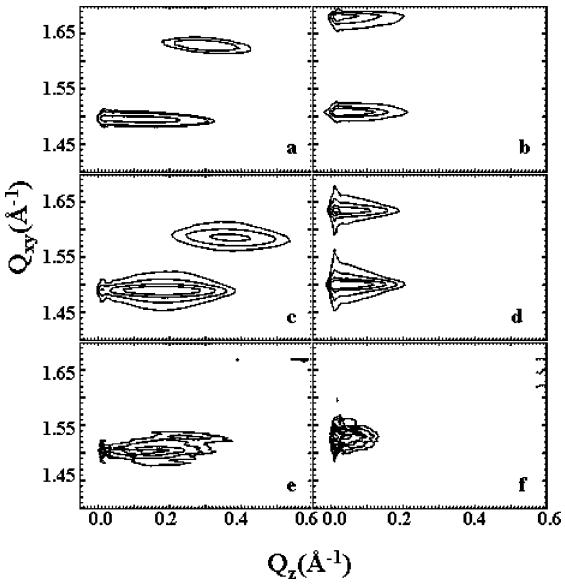

Figure 6. Contour plots of diffracted X-ray intensities as a function of the in-plane component Q_{xy} and the out-of-plane component Q_z of the scattering vector $\boldsymbol{Q}$ of MDO (22-methoxydocosan-1-ol, $H_3C-O-(CH_2)_{22}-OH$): 4 mN·m^{-1} (a) and 10 mN·m^{-1} (b) at 20 °C; 7 mN·m^{-1} (c) and 16 mN·m^{-1}at 26 °C; 4 mN·m^{-1} (e) and 14.8 mN·m^{-1} (f) at 35 °C.

As result, phase diagrams of DME, DO, and MDO have been established in the investigated temperature region (Figure 8). In all cases, the nontilted phases S and LS are observed at high pressure, and L_2' (Ov) is observed as the tilted phase at low pressure. In the case of the monopolar DO and DME, the S/LS phase boundary occurs between 25 and 30 °C. The addition of the second polar group (MDO) shifts this phase boundary to

TABLE 3: Data Derived from GIXD Measurements of MDO between 20 and 35 °C

T (°C)	π (mN m^{-1})	Q_{xy} (Å^{-1})	Q_z (Å^{-1})	*a* (Å)	*b* (Å)	A_0 (Å^2)	A_{xy} (Å^2)	tilt	*d*
20	1	1.610	0.372	5.01	7.81	19.1	19.6	13.0	−0.1058
		1.490	0.186						
	4	1.629	0.284	5.01	7.71	19.0	19.3	9.9	−0.1175
		1.495	0.142						
	7	1.674	0	5.02	7.51	18.9	18.9	0	−0.1465
		1.505	0						
	10	1.675	0	5.02	7.50	18.8	18.8	0	−0.1473
		1.505	0						
	20	1.682	0	5.01	7.47	18.7	18.7	0	−0.1477
		1.511	0						
	30	1.684	0	5.00	7.46	18.6	18.6	0	−0.1475
		1.513	0						
26	2.8	1.548	0.490	4.98	8.11	19.3	20.2	17.6	−0.0608
		1.480	0.244						
	7	1.585	0.373	4.98	7.93	19.2	19.7	13.2	−0.0840
		1.490	0.187						
	11	1.607	0.270	4.98	7.83	19.2	19.5	9.5	−0.0985
		1.495	0.130						
	16	1.635	0	4.99	7.68	19.2	19.2	0	−0.1171
		1.501	0						
	20	1.637	0	4.99	7.68	19.2	19.2	0	−0.1187
		1.501	0						
35	4	1.515	0.388	4.89	8.28	19.6	20.3	14.6	−0.0214
		1.491	0.192						
	7.8	1.525	0.280	4.86	8.33	19.7	20.0	10.4	−0.0222
		1.500	0.140						
	14.8	1.524	0	4.76	8.24	19.6	19.6	0	0

higher temperatures (30−35 °C). This explains why at 20 °C the cross-sectional area of MDO (18.8 Å^2) is smaller than those of DME and DO (19.2 Å^2). At 20 °C, MDO is effectively at a lower temperature (compared with the S/LS transition temperature) than DO and DME, and the cross-sectional area decreases with decreasing temperature. The unit-cell parameters in the cross-section normal to the chains show clearly that the S phase of all samples is characterized by the herringbone packing mode ($a \approx 5$ Å and $b \approx 7.5-7.6$ Å).[42,45−47]

As an example, the full width at half-maximum (fwhm) values of the Bragg peaks of DME are presented in Figure 9. In the L_2' phase, there is a large difference between the fwhm of the degenerated and nondegenerated peaks. The degenerated peaks are much narrower than the nondegenerated peaks. On compression at lower temperature, the tilt angle decreases so that the influence of the tilt fluctuations reduces (Figure 9 top). The difference in fwhm between the two peaks becomes smaller as the surface pressure increases. In the nontilted S phase, the peaks are close to resolution-limited, representing high order in the lattice. The fwhm is linearly decreasing to the small value in the nontilted phase. There is no jump in the fwhm values at the transition pressure. In contrast, at higher temperature, the fwhm difference between the two peaks in L_2' becomes larger with increasing pressure until the nontilted phase is reached. The large fwhm in the S phase at 27 °C (Figure 9 bottom) suggests that this point is already very close to the S/LS phase boundary in the phase diagram. On approaching the S/LS transition, a remarkable loss in positional correlation can be seen, as already described for octadecanol.[41] The monolayers are weakly ordered. In some cases, it is difficult to decide if there are one or two peaks. In a certain temperature interval, the peak of the LS phase is clearly asymmetric and can be treated as two strongly overlapping broad peaks. This has been described as a feature of the LS−rotator I phase.[48] On further increasing temperature, the fwhm again decreases in the LS−rotator II phase. Obviously, the transition from a tilted (L_2' or Ov) into a nontilted phase close to the S/LS boundary is a weak first-order transition. This transition is endothermic. The reason for positive ΔS values might be the very weak ordering in the nontilted compared with the tilted phase. There is clearly a jump of the fwhm at the transition pressure to larger values, explaining the weak first-order endothermic transition.

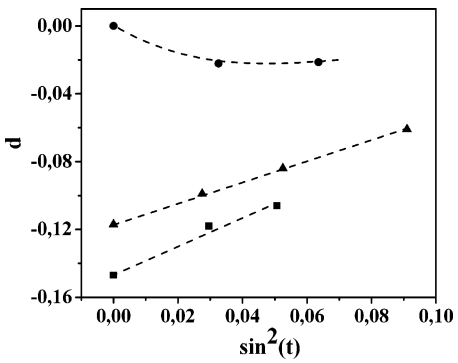

Figure 7. Distortion *d* versus sin^2(*t*), where *t* is the tilt angle to the normal, for MDO (22-methoxydocosan-1-ol, $H_3C-O-(CH_2)_{22}-OH$) at 20 °C (■), 26 °C (▲), and 35 °C (●).

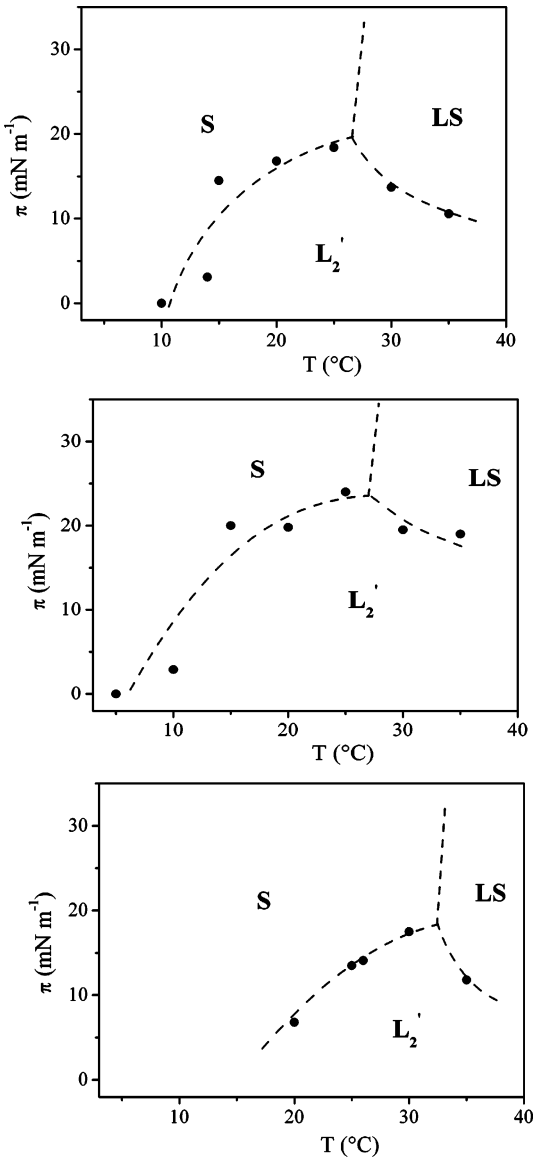

Figure 8. Surface pressure−temperature phase diagrams for monolayers of DME (docosyl methyl ether, $H_3C-(CH_2)_{21}-O-CH_3$) (top), DO (docosan-1-ol, $H_3C-(CH_2)_{21}-OH$) (middle), and MDO (22-methoxydocosan-1-ol, $H_3C-O-(CH_2)_{22}-OH$) (bottom).

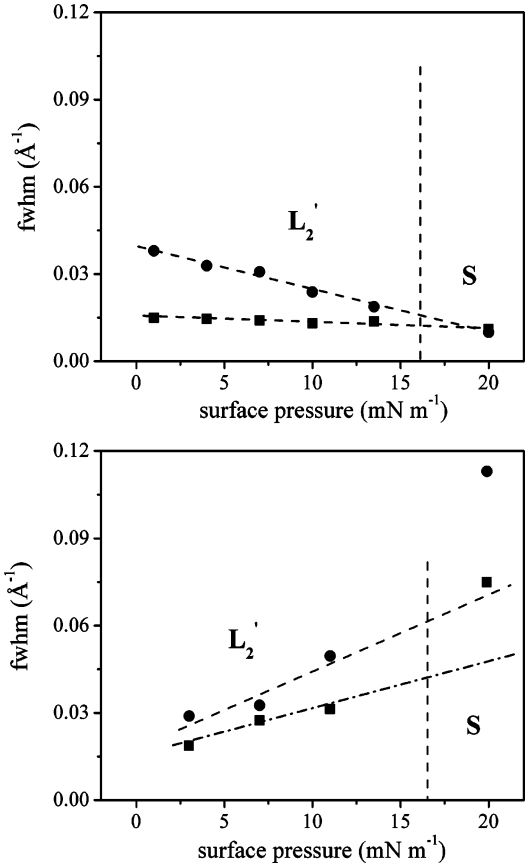

Figure 9. Full-width at half-maximum (fwhm) of the Bragg peaks (▲ = nondegenerate peak, ■ = degenerate peak) of DME (docosyl methyl ether, $H_3C-(CH_2)_{21}-O-CH_3$) at 20 °C (top) and 27 °C (bottom) as function of surface pressure.

In summary, the additional second polar group did not change the general phase sequence and the lattice structure, but it leads only to a shift of the phase boundaries.

3.3. XPS Measurements. An XPS TOA dependency experiment was made to clarify the endgroup orientation in the bipolar MDO monolayer transferred onto solid support at 27 mN·m^{-1} and 20 °C. Under these conditions, GIXD measurements have shown that the film molecules are completely upright oriented in a well-ordered S phase. Figure 10 presents the XPS spectra of C1s for the MDO monolayer obtained at TOAs between 5° and 80°. Two peaks are clearly resolved at 284.6 eV and 286.2−286.3 eV, which are attributed to C1s photoelectrons from C−H in the alkyl chain and from C−O in the terminal hydroxyl and/or methoxy groups, respectively.[49] The area fraction of the elements is plotted with respect to TOA in Figure 11, to show the relative contribution of the photoelectrons to the total C1s intensity. The plot shows that the C−O contribution increases at low TOAs. This indicates that at least one of the polar end groups is exposed to the air, although it is not clear which of the two polar end groups is the outward one.

According to wettability studies of self-assembled monolayers of derivatized alkanthiols having terminally functionalized alkyl chains, the contact angles of −OH and $-OCH_3$ terminated monolayers against water are 0° and 74°, respectively.[50] According to the Young−Dupre equation, the contact angle θ is related to adhesion energy W_a and liquid/vapor interfacial tension γ_{LV} by $W_a = \gamma_{LV}(1 + \cos\theta)$. The above-mentioned contact angle data implies that the hydroxyl group is more hydrophilic and more adhesive to water in comparison to the methoxy group. Therefore, we conclude that the methoxy group

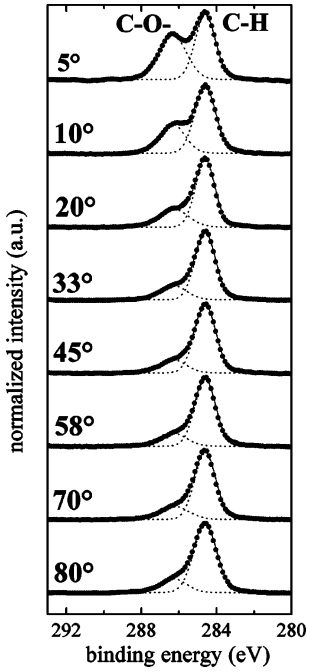

Figure 10. TOA dependence of XPS C1s spectra for MDO (22-methoxydocosan-1-ol, $H_3C-O-(CH_2)_{22}-OH$) monolayer on Si wafer.

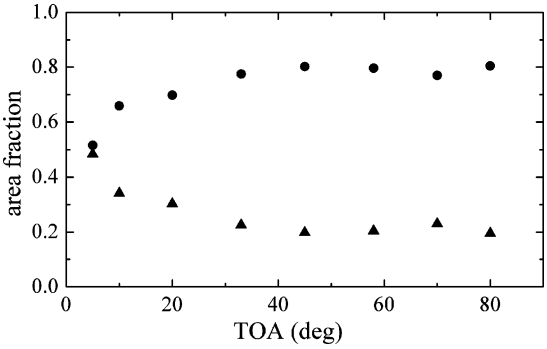

Figure 11. Percentage area of C−H (●) and C−O− (▲) as function of TOA for MDO (22-methoxydocosan-1-ol, $H_3C-O-(CH_2)_{22}-OH$) monolayer on Si wafer.

of MDO points to the air and the hydroxyl group is attached to the water surface.

4. Conclusion

New mono- and bipolar single-chain amphiphiles (MDO and DME) were synthesized, and their monolayer behavior at the air/water interface was studied in comparison with DO using pressure−area isotherms and grazing incidence X-ray diffraction in the temperature region between 15 and 35 °C. All monolayers are fully condensed with a phase transition from the tilted centered rectangular L_2' to the nontilted orthorhombic S phase at lower temperature or the nontilted hexagonal LS phase at higher temperature. Both headgroups allow the same tight packing of the molecules in monolayers. Inserting the second polar group (mono- to bipolar molecules) does not change the phase behavior qualitatively. However, the second polar group is responsible for shifting the S/LS boundary to higher temperatures. The small plateau in the isotherms at higher temperatures close to or above the S/LS boundary is characteristic for a weak endothermic first-order phase transition. The reason that the transition is endothermic might be the observed decrease in the positional order in the nontilted phase compared with the tilted phase below the transition pressure. An endothermic process

has also been observed in monolayers of octadecylureas.[51] However, in this case, the hydrogen-bond network among the urea headgroups was the reason for the anomalous phase transition accompanied by area contraction with increasing temperature at constant pressure.

XPS supports the model that the more hydrophilic hydroxyl group of the bipolar compound is attached to the water. Since the methoxy group is obviously less hydrophilic, it is pointing to the hydrophobic air. The energetic disadvantage due to such orientation is compensated by other interactions such as strong adhesive force of the hydroxyl group with water and van der Waals interaction between the long alkyl chains in the densely packed monolayer. These strong van der Waals interactions between the long hydrocarbon chains together with the weak hydrophilicity of the methoxy group might also be the reason that there is no indication of any transition from a state where both headgroups are attached to the water surface to a state where only one hydrophilic headgroup remains attached to the water. Obviously, the self-aggregation into a condensed phase with almost upright oriented molecules already occurs during the spreading process.

Acknowledgment. This work was supported by the Max Planck Society (X.Y.), the Alexander von Humboldt Foundation (K.I.), and the Venture Business Laboratory at Utsunomiya University (G.B.). The help of Kristian Kjaer with setting up the X-ray experiment is gratefully acknowledged. We thank HASYLAB at DESY, Hamburg, Germany, for beam time and providing excellent facilities and support.

References and Notes

(1) Shih, M. C.; Bohanon, T. M.; Mikrut, J. M.; Zschack, P.; Dutta, P. *J. Chem. Phys.* **1992**, *97*, 4485.
(2) Lautz, C.; Fischer, T. M. *J. Phys. Chem. B* **1997**, *101*, 8790.
(3) Lautz, C.; Fischer, T. M.; Kildae, J. *J. Chem. Phys.* **1997**, *106*, 7448.
(4) Lautz, C.; Fischer, T. M.; Weygand, M.; Lösche, M.; Howes, P. B.; Kjaer, K. *J. Chem. Phys.* **1998**, *108*, 4640.
(5) Brezesinski, G.; Kaganer, V. M.; Möhwald, H.; Howes, P. B. *J. Chem. Phys.* **1998**, *109*, 2006.
(6) Kaganer, V. M.; Brezesinski, G.; Möhwald, H.; Howes, P. B.; Kjaer, K. *Phys. Rev. Lett.* **1998**, *81*, 5864.
(7) Kaganer, V. M.; Brezesinski, G.; Möhwald, H.; Howes, P. B.; Kjaer, K. *Phys. Rev. E* **1999**, *59*, 2141.
(8) Teer, E.; Knobler, C. M.; Lautz, C.; Wurlitzer, S.; Kidae, J.; Fischer, T. M. *J. Chem. Phys.* **1997**, *106*, 1913.
(9) Fuhrhop, J.-H.; Wang, T. *Chem. Rev.* **2004**, *104*, 2901.
(10) Menger, F. M.; Richardson, S. D.; Wood, M. G.; Sherrod, M. J. *Langmuir* **1989**, *5*, 833.
(11) Overs, M.; Fix, M.; Jacobi, S.; Chi, L. F.; Sieber, M.; Schäfer, H.-J.; Fuchs, H.; Galla, H.-J. *Langmuir* **2000**, *16*, 1141.
(12) Woese, C. R.; Fox, G. E. *Proc. Natl. Acad. Sci. U.S.A.* **1977**, *74*, 5088.
(13) Woese, C. R.; Kandler, W.; Wheelis, M. L. *Proc. Natl. Acad. Sci. U.S.A.* **1990**, *87*, 4576.
(14) Langworthy, T. A. *Biochim. Biophys. Acta* **1977**, *487*, 37.
(15) DeRosa, M.; Gambacorta, A. *Prog. Lipid Res.* **1988**, *27*, 153.
(16) Gulik, A.; Luzatti, V.; DeRosa, M.; Gambacorta, A. *J. Biol. Chem.* **1985**, *183*, 131.
(17) DeRosa, M.; Gambacorta, A.; Gliozzi, A. *Microbiol. Rev.* **1986**, *50* (1), 70.
(18) Gambacorta, A.; Gliozzi, A.; DeRosa, M. *World Microbiol. Biotechnol.* **1995**, *11*, 115.
(19) Bauer, S.; Heckmann, K.; Six, L.; Strobl, C. *Desalination* **1983**, *46*, 369.
(20) Ring, K.; Henkel, B.; Valenteijn, A.; Gutermann, R. In L*iposomes as Drug Carriers*; Schmidt, K. H., Ed.; Georg Thieme Verlag: Stuttgart, 1986; pp 100−123.
(21) Fuhrhop, J.-H.; David, H. H.; Mathieu, J.; Liman, U.; Winter, H. J.; Boeckema, E. *J. Am. Chem. Soc.* **1986**, *108*, 1785.
(22) Fuhrhop, J.-H.; Krull, M.; Schulz, A.; Möbius, D. *Langmuir* **1990**, *6*, 497.
(23) Böhme, P.; Hicke, H.-G.; Boettcher, C.; Fuhrhop, J.-H. *J. Am. Chem. Soc.* **1995**, *117*, 5824.
(24) Dante, S.; Pouzi-Bossi, M. G.; Rustichelli, F. In *Electrical and Related Properties of Organic Solids*; Munn, R. W. et al., Eds.; 1997; pp 431−443.
(25) DeRosa, M. *Thin Solid Films* **1996**, *284*−*285*, 13.
(26) Di Meglio, C.; Rananavare, S. B.; Svenson, S.; Thompson, D. H. *Langmuir* **2000**, *16*, 128.
(27) Bakowsky, U.; Rothe, U.; Antonopoulos, E.; Martini, T.; Henkel, L.; Freisleben, H.-J. *Chem. Phys. Lipids* **2000**, *105*, 31.
(28) Laggner, P.; Lohner, K.; Degovics, G.; Müller, K.; Schuster, A. *Chem. Phys. Lipids* **1987**, *44*, 31.
(29) Brezesinski, G.; Dietrich, A.; Struth, B.; Böhm, C.; Bouwman, W. G.; Kjaer, K.; Möhwald, H. *Chem. Phys. Lipids* **1995**, *76*, 145.
(30) Maruyama, S.; Matsuki, H.; Ichimori, H.; Kaneshina, S. *Chem. Phys. Lipids* **1996**, *82*, 125.
(31) Fix, M.; Lauter, R.; Lobbe, C.; Brezesinski, G.; Galla, H.-J. *Langmuir* **2000**, *16*, 8937.
(32) Fix, M.; Wiehle, S.; Haufe, G.; Galla, H.-J. *Colloids Surf., A* **2002**, *198*−*200*, 151.
(33) Heiser, U. F.; Dobner, B. *Chem. Commun.* **1996**, *17*, 2025.
(34) Heiser, U. F.; Dobner, B. *J. Chem. Soc., Perkin Trans. 1* **1997**, 809.
(35) Hazell, L. B.; Rizivi, A. A.; Brown, I. S.; Ainsworth, S. *Spectrochim. Acta, Part B* **1985**, *40*, 739.
(36) Jacquemain, D.; Leveiller, F.; Weinbach, S. P.; Lahav, M.; Leiserowitz, L.; Kjaer, K.; Als-Nielsen, J. *J. Am. Chem. Soc*. **1991**, *113*, 7684.
(37) Kjaer, K. *Physica B* **1994**, *198*, 100.
(38) Als-Nielsen, J.; Jacquemain, D.; Kjaer, K.; Leveiller, F.; Lahav, M.; Leiserowitz, L. *Phys. Rep.* **1994**, *246*, 252.
(39) Majewski, J.; Popovitz-Biro, R.; Bouwman, W. G.; Kjaer, K.; Als-Nielsen, J.; Lahav, M.; Leiserowitz, L. *Chem.*−*Eur. J.* **1995**, *1*, 304.
(40) Brezesinski, G.; Dietrich, A.; Struth, B.; Böhm, C.; Bouwman, W. G.; Kjaer, K., Möhwald, H. *Chem. Phys. Lipids* **1995**, *76*, 145.
(41) Jensen, T. R.; Kjaer, K. In *Novel Methods to Study Interfacial Layers, Studies in Interface Science*; Moebius, D., Miller, R., Eds.; Elsevier Sciences B. V.: Amsterdam, 2001; Vol. 11, pp 205−254.
(42) Kaganer, V. M.; Brezesinski, G.; Möhwald, H.; Howes, P. B.; Kjaer, K. *Phys. Rev. Lett.* **1998**, *81*, 5864.
(43) Kaganer, V. M.; Möhwald, H.; Dutta, P. *Rev. Mod. Phys.* **1999**, *71*, 779.
(44) Brezesinski, G.; Kaganer, V. M.; Möhwald, H.; Howes, P. B. *J. Chem. Phys.* **1998**, *109*, 2006.
(45) Kitaigorodskii, A. I. *Organic Chemical Crystallography*; Consultants Bureau: New York, 1961.
(46) Durbin, M. K.; Richter, A.; Yu, C.-J.; Kmetko, J.; Bai, J. M.; Dutta, P. *Phys. Rev. E* **1998**, *58*, 7686.
(47) Kuzmenko, I. V.; Kaganer, V. M.; Leiserowitz, L. *Langmuir* **1998**, *14*, 3882.
(48) Shih, M. C.; Bohanon, T. M.; Mikrut, J. M.; Zschack, P.; Dutta, P. *Phys. Rev. A* **1992**, *45*, 5734.
(49) Wagner, C. D.; Riggs, W. M.; Davis, L. E.; Moulder, J. F.; Muilenberg, G. E. In *Handbook of X-ray Photoelectron Spectroscopy*; Chastain, J., Ed.; Perkin-Elmer Corp., Physical Electronics Division, Minnesota, 1979.
(50) Bain, C. D.; Troughton, E. B.; Tau, Y. T.; Evall, J.; Whitesides, G. M.; Nuzzo, R. G. *J. Am. Chem. Soc.* **1989**, *111*, 321.
(51) Shimizu, M.; Yoshida, M.; Iimura, K.; Suzuki, N.; Kato, T. *Colloids Surf., A* **1995**, *102*, 69.